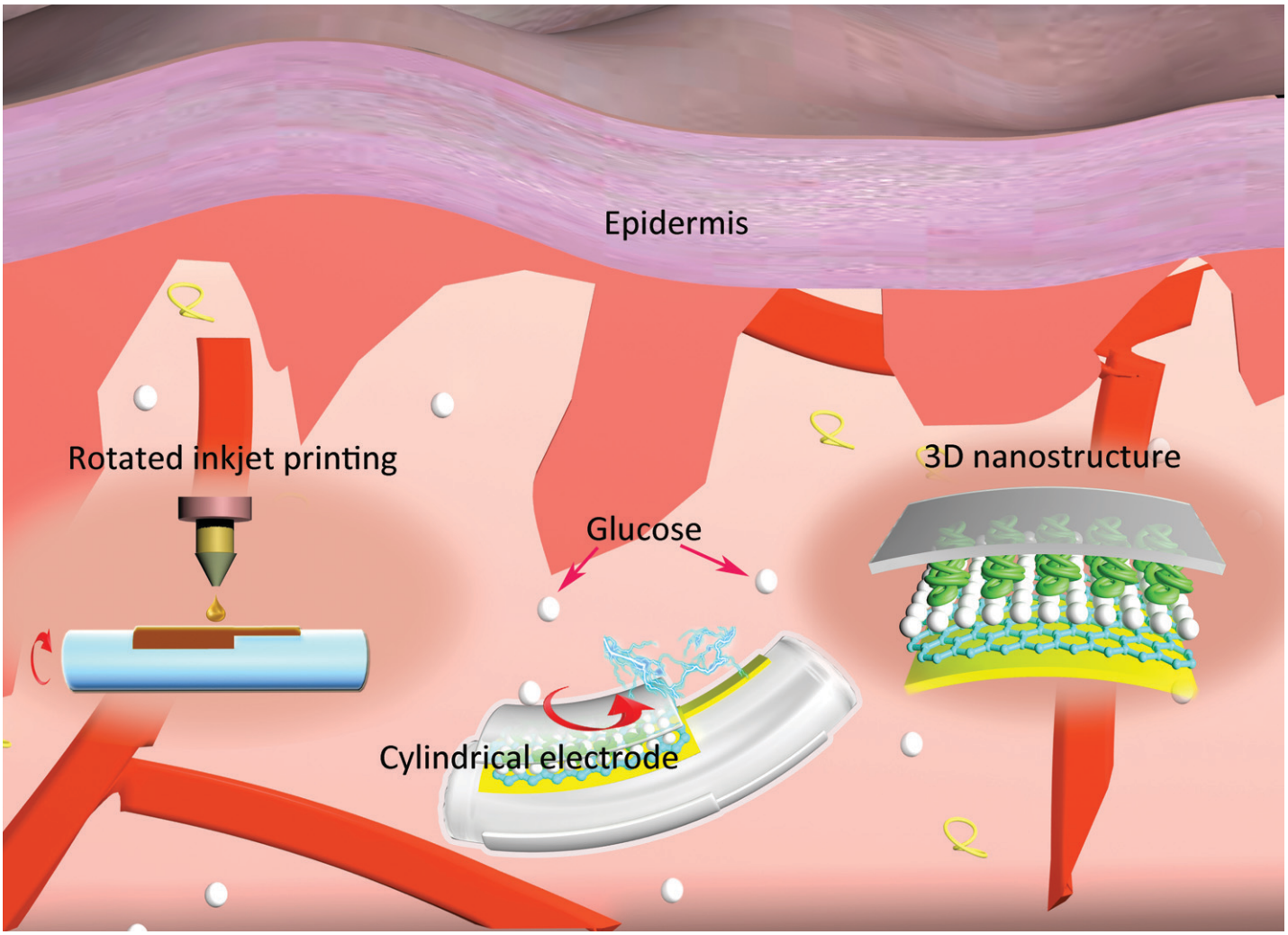

Featuring work from Dachao Li's group at the State Key Laboratory of Precision Measuring Technology and Instruments, Tianjin University, China.

A flexible enzyme-electrode sensor with cylindrical working electrode modified with a 3D nanostructure for implantable continuous glucose monitoring

A novel cylindrical flexible enzyme-electrode sensor was fabricated with a big working electrode surface for implantable continuous glucose monitoring. A rotated inkjet printing method was proposed to fabricate the electrodes and construct a 3D nanostructure on the micro cylindrical substrate.

As featured in:

See Haixia Yu, Dachao Li *et al.*, *Lab Chip*, 2018, **18**, 3570.

ROYAL SOCIETY OF CHEMISTRY

rsc.li/loc

Registered charity number: 207890

Lab on a Chip

PAPER

View Article Online
View Journal | View Issue

Cite this: *Lab Chip*, 2018, **18**, 3570

A flexible enzyme-electrode sensor with cylindrical working electrode modified with a 3D nanostructure for implantable continuous glucose monitoring†

Zhihua Pu, [a] Jiaan Tu,[a] Ruixue Han,[b] Xingguo Zhang,[a] Jianwei Wu,[a] Chao Fang,[a] Hao Wu,[a] Xiaoli Zhang,[a] Haixia Yu*[b] and Dachao Li*[a]

A novel cylindrical flexible enzyme-electrode sensor was fabricated with a bigger working electrode (WE) surface than the traditional pin-like one for implantable continuous glucose monitoring. On the WE surface, a 3D nanostructure consisting of graphene and platinum nanoparticles was constructed to enhance the sensitivity; in conjunction with the bigger WE, this nanostructure enabled hypoglycemia detection, which is still a big challenge in clinics. The cylindrical sensor was fabricated by rotated inkjet printing which enabled direct patterning of microstructures on a curved surface, thus overcoming the restriction of the traditional planar micromachining by photolithography. Specifically, the cylindrical substrate (polyetheretherketone, PEEK) was modified by (3-aminopropyl) trimethoxysilane and (3-mercaptopropyl) trimethoxysilane to facilitate surface wettability, which discourages the coalescence of adjacent droplets, and to facilitate the adhesion of metals to PEEK in order to construct robust electrodes. A synchronous heating method was used to evaporate the solvent of the droplets quickly to prevent them from running along the cylindrical surface, which affects the formation of the printed electrode significantly. *In vitro* experimental results showed that the proposed sensor was able to detect the glucose concentration ranging from 0 to 570 mg dL^{-1} which demonstrated its capability for physiological glucose detection. *In vivo* experiments were conducted with rats, and the measurement results recorded using the implanted cylindrical sensor showed great compliance to those recorded using a commercial glucometer which exhibited the viability of the proposed sensor for implantable continuous glucose monitoring, even under the hypoglycemic conditions.

Received 28th August 2018,
Accepted 17th October 2018

DOI: 10.1039/c8lc00908b

rsc.li/loc

Introduction

Diabetes mellitus and its complications have become great health risks to humans.[1,2] Continuous blood glucose monitoring is considered the best method to reveal the illness state of diabetics in order to help effectively control diabetes and its complications.[3] However, continuous and direct monitoring of glucose in the blood still has many difficulties.[4] Thus, continuous blood glucose prediction based on interstitial fluid (ISF) analysis has attracted much attention because the glucose concentrations in the ISF are closely related to those in the blood.[5,6] To date, the use of implantable enzyme-electrode sensors is still the most frequently used ISF analysis method for clinical continuous glucose monitoring.[7] Unfortunately, the rigid pin-like structure (needle-type and coil-type) of traditional enzyme-electrode sensors cannot make stable contact with the subcutaneous tissue, which may lead to signal drift.[8] Moreover, this kind of implantable sensor requires a minute diameter so that the area of the effective working electrode (WE) is very small because it is usually manufactured on the cylindrical end face. The small WE area leads to a low sensitivity of the sensor. Therefore, it is hard for traditional enzyme-electrode sensors to realize hypoglycemia detection, which is as yet a significant challenge for clinical continuous glucose monitoring.[9] In this paper, a novel cylindrical flexible enzyme-electrode sensor with a bigger WE surface is proposed for implantable continuous glucose monitoring to avoid signal drift and enable hypoglycemia detection. A cylindrical substrate is selected because it holds the biggest surface compared with the other shapes for a certain volume, and a bigger cylindrical surface produces a bigger WE surface. And on a cylindrical surface, the WE not only can be fabricated along the radius but also along the axis of the

[a] *State Key Laboratory of Precision Measuring Technology and Instruments, Tianjin University, Tianjin 300072, China. E-mail: dchli@tju.edu.cn*
[b] *Tianjin Key Laboratory of Biomedical Detecting Techniques and Instruments, Tianjin University, Tianjin 300072, China. E-mail: hxy2081@tju.edu.cn*

† Electronic supplementary information (ESI) available. See DOI: 10.1039/c8lc00908b

cylindrical substrate breaking through the limit of the diameter which exists for traditional pin-like enzyme-electrode sensors.

Nowadays, patterning on a micro cylindrical substrate still has many difficulties.[10] The traditional lithography micromachining method exhibits excellent performance for patterning on an *a* plane but not for a curved surface; and this limitation hinders its application to cylindrical substrates. Choi *et al.* employed a soft mask of polydimethylsiloxane film to fit the surface to enable the fabrication of submicron patterns on curved substrates.[11] However, the difficulties involved in uniformly coating a photoresist on a curved surface are yet to be overcome to meet the requirements of photolithography. Petruczok *et al.* proposed a soft-lithography method based on initiated chemical vapor deposition to enable the patterning of functional organic surfaces and metal microstructures on cylindrical substrates.[12] Wang *et al.* used a reusable, flexible and low cost parylene-C/Cr shadow mask to enable the fabrication of diverse micro patterns on arbitrary surfaces.[13] The two methods enable patterning on a curved surface while the difficult mask manipulation (former method) and the hard transfer operation (latter one) make them only suitable for structure patterning on a side of a micro cylindrical substrate, leading to the insufficient use of the whole surface area. A higher surface utilization rate facilitates the miniaturization of devices which holds great significance for implantable devices. In addition, multilayer microstructure fabrication is hard to achieve based on the two methods due to the difficulty of alignment. Sun *et al.* used a confined evaporative self-assembly method to fabricate tubular structures containing conductive stripe patterns on flexible polyimide films which could be rolled up to make 3D tubular cell complexes.[14] This method enables patterning on a curved surface but it is restricted to cycle's manufacturing and it is difficult to control the shape of the patterning. All of the aforementioned methods have difficulty fabricating multilayer microstructures on a whole micro cylindrical substrate.

Inkjet printing is an additive manufacturing technique that has been used in various fields such as wearable electronics,[15] optoelectronics,[16] transducers,[17] microfluidics,[18] and energy devices[19] owing to its inherent advantages. This method poses no limit over the shape of the substrate, which exhibits the possibility of fabrication on cylindrical substrates.[20] Furthermore, this technology enables maskless direct writing which avoids difficult mask manipulation for curved surfaces and enables multilayer structure patterning especially for *in situ* fabrication and modification on a whole micro cylindrical substrate.[21] The maskless method also avoids the development process and saves time and materials which results in a low cost.[22] Additionally, this technique enables low temperature fabrication which is beneficial in maintaining the bioactivity of graphically deposited biomaterials, which is of importance to biosensors.[23] Therefore, in this paper, a novel rotated inkjet printing method is proposed to enable facile micromanufacturing of multilayer microstructures on a whole micro cylindrical substrate to form flexible glucose sensors.

Experimental

Chemicals and materials

The cylindrical flexible substrate (polyetheretherketone, PEEK, diameter: 1 mm, the length of the fabricated sensor: 5 mm, stiffness: 62.5 kN m^{-1}) was purchased from Shenzhen Xiangping Insulating Materials Co., Ltd., Shenzhen, China. (3-Aminopropyl) trimethoxysilane (APTES), (3-mercaptopropyl) trimethoxysilane (MPTMS), glucose oxidase (GOx), silver ink, graphene ink and Nafion were all bought from Sigma-Aldrich LLC., Shanghai, China. Gold ink was obtained from Ptdots, Inc., USA. Platinum nanoparticle (PtNP) ink was obtained from Changchun Institute of Applied Chemistry Chinese Academy of Sciences, China. Ferric chloride ($FeCl_3$), glucose, potassium ferricyanide, hydrogen peroxide (H_2O_2, 30 wt%), 0.1 M phosphate buffered saline (PBS) solution (pH = 7.4) and absolute ethyl alcohol were all bought from Tianjin Jiangtian Huagong Co., China. Urethane and glucose injection were supported by the Animal Experiment Center of the Chinese Academy of Medical Sciences & Peking Union Medical College Institute of Biomedical Engineering, Tianjin, China. All of the chemicals were used as received without any purification.

Surface modification of the PEEK rod

The commercial solutions of APTES and MPTMS were respectively diluted in ethanol by 10% and 1% per volume, and then the two diluted solutions were mixed 1 : 1 (v/v). Before decorating with APTES and MPTMS, the cylindrical PEEK rod was pretreated using O_2 plasma for 1 min to obtain an activated surface which was beneficial for the modification. Then, the PEEK rods were immersed into the mixture for 2 h to accomplish surface functionalization, followed by rinsing with ethanol and drying in the nitrogen stream.

Fabrication of the cylindrical flexible enzyme-electrode sensor

The cylindrical flexible enzyme-electrode glucose micro sensor was fabricated *via* rotated inkjet printing. This rotated inkjet printing system is shown in Fig. S1.† The cylindrical flexible PEEK rod substrate was clutched by a tripod chuck on a rotary motor after surface modification. Subsequently, the displacement stage and the rotary motor were maneuvered according to the predefined printing tracks. And the heater worked simultaneously (~200 °C, ~2 mm to the rod surface) during all printing processes except for GOx. For the electrode printed materials, gold ink, graphene ink, and PtNP ink were utilized for the WE; silver ink was utilized for the CE and RE. After each electrode layer was fabricated, they were annealed (350 °C for 30 min for Au and graphene, 350 °C for 10 min for Ag, ~2 mm between the heater and the rod surface) to enhance the conductivity of the printed microelectrodes. After heating, the electrodes were immersed in 50 mM $FeCl_3$ aqueous solution for 50 s to obtain a stable Ag/AgCl CE and RE, then 10 μL Nafion solution was dropped onto the electrode surface to

produce a covering layer in order to make them more biocompatible and more stable in an interstitial environment.[24] After that, PtNPs were ejected onto the annealed graphene layer, GOx was printed onto the WE surface at room temperature and immobilized with Nafion, and a cylindrical flexible enzyme-electrode glucose sensor was obtained.

Characterization of the fabricated cylindrical flexible sensor

All of the electrochemical measurements were performed on an electrochemical workstation (CHI 660E, CH Instruments, Ins., USA). *In vitro* experiments were conducted to characterize the printed cylindrical flexible electrochemical sensor using cyclic voltammetry, chronoamperometry and electrochemical impedance spectroscopy. *In vivo* experiments were conducted by implanting the proposed sensor into the subcutaneous tissue of a rat, and the detection method was chronoamperometry.

In vivo animal experiment

Eight healthy SD rats were purchased from Beijing Vital River Laboratory Animal Technology Co., Ltd. The rat used in the experiment was fasted for 8 h before the test. Urethane (0.7 g kg^{-1}) was first used to anesthetize the rat by intraperitoneal injection. Then, the fabricated cylindrical flexible sensor was implanted into the subcutaneous tissue of the rat's posterior neck after complete narcosis. After a period of 30 min, the amperometric method was used to record the data from the implanted sensor continuously using a commercial glucometer (OneTouch®, LifeScan, Inc., USA) to measure the caudate blood glucose of the rat every 10 min. After 30 min

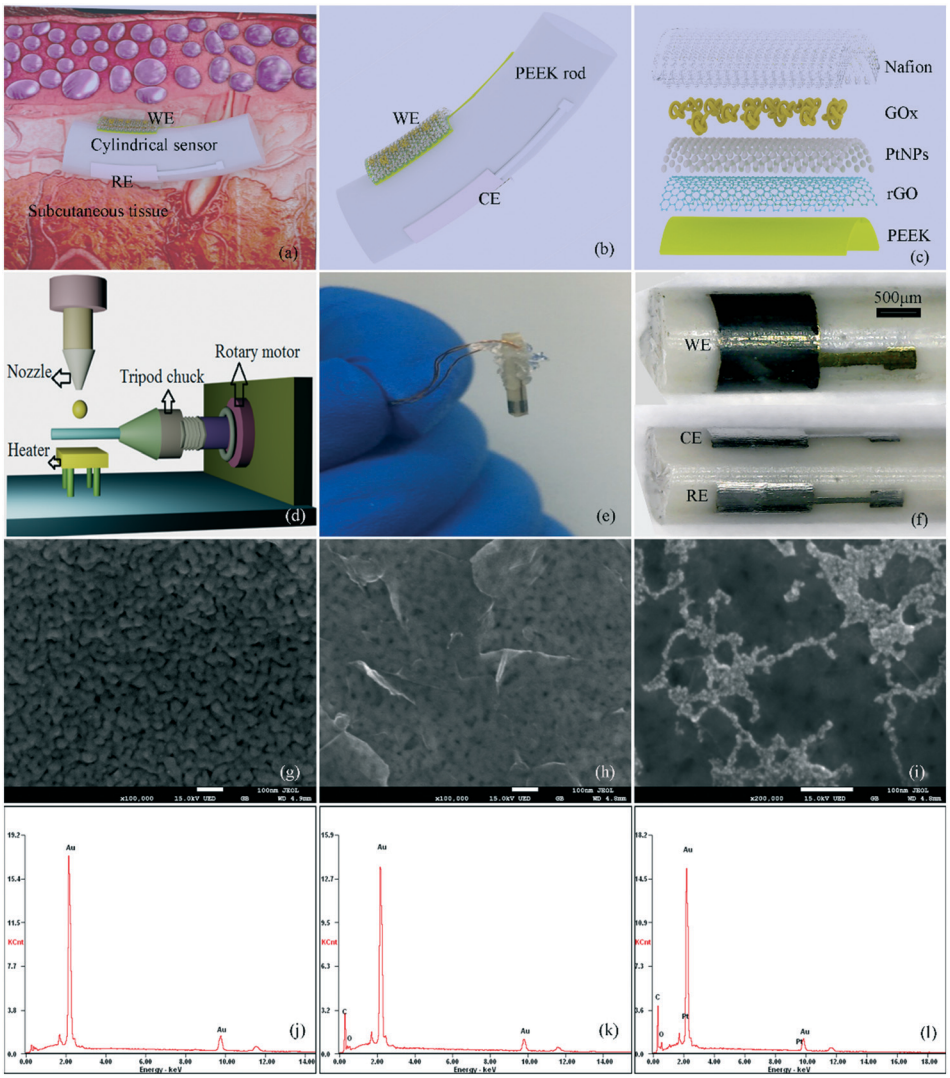

Fig. 1 Schematic diagrams and photos of the cylindrical flexible enzyme-electrode glucose sensor. (a) Implantable application of the flexible sensor in the subcutaneous tissue; (b) structure of the cylindrical enzyme-electrode glucose sensor; (c) structure of the WE; (d) the rotated inkjet printing system for manufacturing the cylindrical sensor; (e) photo of the fabricated sensor; (f) photo of the three electrodes of the cylindrical sensor; (g) SEM image of the Au WE surface; (h) SEM image of the rGO/Au WE surface; (i) SEM image of the PtNP/rGO/Au WE surface; (j) EDS of the Au WE surface; (k) EDS of the rGO/Au WE surface; (l) EDS of the PtNP/rGO/Au WE surface.

of monitoring, glucose (20 g kg^{-1}) was injected into the abdomen of the rat. Then, detection occurred for about 4 h. Eight fabricated sensors were used for the eight rats. All of the data collected were then analysed.

Results and discussion

Formation of the cylindrical enzyme-electrode glucose sensor

Fig. 1(a) shows the concept diagram of the proposed cylindrical enzyme-electrode sensor implanted in the subcutaneous tissue to enable real-time glucose detection. The proposed device is a three-electrode electrochemical sensor fabricated on the cylindrical surface of a flexible micro rod. As demonstrated in Fig. 1(b), the cylindrical enzyme-electrode sensor consists of a flexible cylindrical substrate (PEEK rod), a WE, an Ag/AgCl reference electrode (RE), an Ag/AgCl counter electrode (CE), and a Nafion protective membrane. The detailed structure of the WE is displayed in Fig. 1(c), including the flexible cylindrical substrate, the gold layer, the 3D nanostructure consisting of reduced graphene oxide (rGO), PtNPs, the GOx layer, and the Nafion layer. The cylindrical sensor has a bigger WE surface than the traditional pin-like one, and a bigger WE surface is beneficial for the collection of measurement signals especially for the weak signals, for example, the weak current signals associated with low levels of glucose. Furthermore, the flexibility of the sensor enables it to adaptively conform to the deformation of the subcutaneous tissue; the good contact generates more stable detection signals.[25] The stability benefits the analysis of weak useful signals. Additionally, the 3D nanostructure is constructed on the WE to enhance the sensitivity in order to achieve glucose detection at low levels.[26] These three advantages exhibit the potential of the cylindrical flexible enzyme-electrode glucose sensor for hypoglycemia detection.

As illustrated in Fig. 1(d) and S1,† a rotated inkjet printing system was used to fabricate the designed cylindrical glucose sensor. The photos of the fabricated sensor are shown in Fig. 1(e) and (f). The topographies of each layer of the WE surface were characterized using a field emission scanning electron microscope (SEM); the SEM images for each WE configuration of Au, rGO/Au, and PtNPs/rGO/Au are shown in Fig. 1(g)–(i), respectively. The energy dispersive spectroscopy (EDS) spectra for all of the WE configurations are displayed in Fig. 1(j)–(l), respectively. The element ratio for the electrode of PtNPs/rGO/Au is shown in Table 1. These results indicate that the 3D nanostructure consisting of graphene and PtNPs is successfully constructed on the WE surface.

Table 1 Element ratio for the WE of PtNPs/rGO/Au

Element	Au	C	O	Pt
wt%	75.83	18.98	2.88	2.32

Surface modification of PEEK and synchronous heating for electrode manufacturing

The flexible PEEK rod (1 mm) was selected as the cylindrical substrate owing to its excellent physicochemical stability and good biocompatibility.[27] Moreover, this material maintains its properties even at elevated temperatures, which is of importance for annealing the ejected microstructures. Unfortunately, although the rotated inkjet printing method exhibits viability for micromanufacturing on cylindrical surfaces, many plastic materials, for example PEEK, show hydrophobicity and poor adhesion to metals. The hydrophobicity of PEEK inhibits the dispersion of the ejected ink droplets on the surface; this phenomenon leads to corresponding coalescence of adjacent droplets and thus causes long evaporation time for the ink solvent.[28] Poor adhesion to metals hinders durable electrode formation on the PEEK rod substrate. If the printed electrodes are not strongly bonded to the substrate, they may easily fall off from the rod under applied voltage, pressure or liquid immersion. Therefore, as demonstrated in Fig. 2(a), in order to overcome these hurdles, we decorated the PEEK rode substrate surface with APTES and MPTMS. APTES was used to couple ($-NH_2$) to the PEEK substrate to promote the surface wettability, which facilitated the droplet dispersion thus avoiding coalescence with adjacent droplets. MPTMS was used to couple (–SH) to the PEEK substrate to promote the adhesion of metals to PEEK, which was beneficial for constructing robust electrodes on the PEEK rod surface.[29]

Raman spectroscopy of the PEEK rod surface after modification is shown in Fig. 2(b). It can be clearly seen that peaks exist near 3100 cm^{-1} and 800 cm^{-1} for $-NH_2$ bending and –SH stretching, respectively, which verifies the successful surface modification of $-NH_2$ and –SH. After modification, microstructures were fabricated on the cylindrical surface under different conditions; the photos obtained from the observation module are illustrated in Fig. 2. Fig. 2(c) shows the printed results on the cylindrical substrate without modification; corresponding coalescence of contiguous droplets due to the hydrophobic surface is clearly exhibited. The results showed no difference whether heating was applied during printing or not. The printed result for the substrate with surface modification and without synchronous heating is shown in Fig. 2(d). From this photo, we can easily find that the surface became hydrophilic by modification, as the droplets run along the surface under gravity, and in the direction of the centrifugal force during rotation; flowing significantly affects the electrode formation. Thus, we used synchronous heating during printing to evaporate the solvent of the ejected droplets quickly to hinder their flowing; then the printed result is shown in Fig. 2(e) which exhibits a regular shape for microstructure manufacturing. In order to verify robust adhesion between the substrates and printed microelectrodes, a water bath ultrasound test was used. Fig. 2(e) and (f) show the photos of the printed microelectrodes on the flexible cylindrical substrate with and without surface modification,

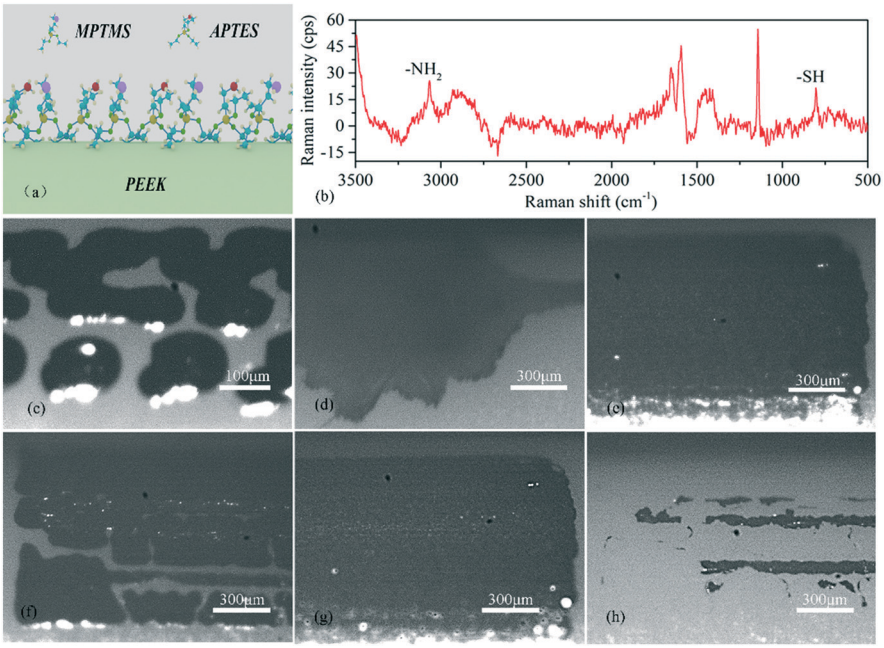

Fig. 2 Surface modification of the PEEK rod and synchronous heating for microelectrode manufacturing. (a) Schematic of the surface modification of PEEK by APTES and MPTMS; (b) Raman spectroscopy of PEEK with surface modification; (c) photo of the microelectrode printed on the substrate without modification; (d) photo of the microstructure printed on the substrate with surface modification and ejected without synchronous heating; (e) photo of the microelectrode printed on the substrate with surface modification and ejected with synchronous heating before water bath ultrasound treatment; (f) photo of the microelectrode printed on the substrate without surface modification and ejected with synchronous heating before ultrasound treatment; (g) photo of the microelectrode printed on the substrate with surface modification and ejected with synchronous heating after ultrasound treatment; (h) photo of the microelectrode printed on the substrate without surface modification and ejected with synchronous heating after ultrasound treatment.

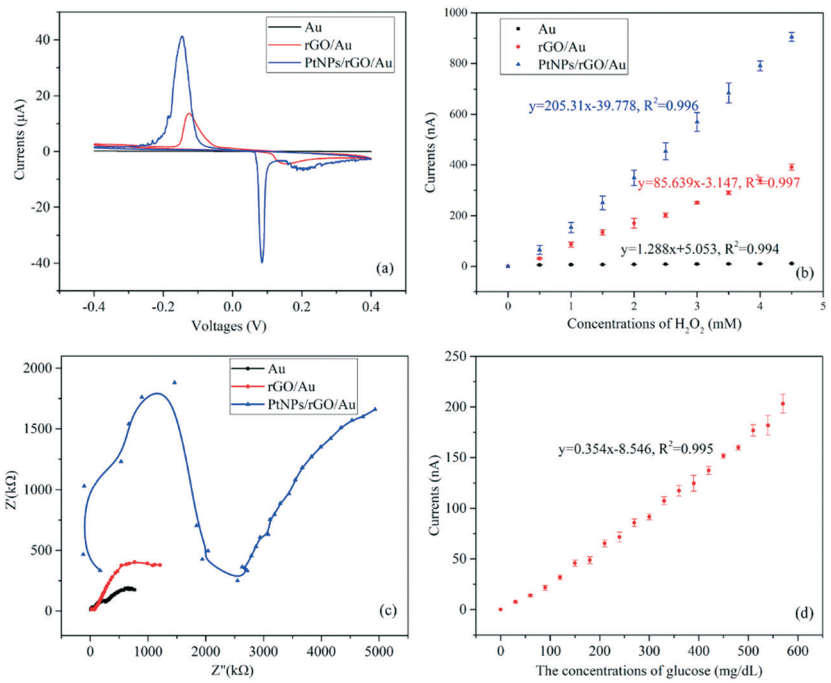

Fig. 3 Electrochemical characterization of the printed cylindrical flexible sensors. (a) Cyclic voltammetry curves to 0.1 mM PBS containing 1 mM H_2O_2 by the different configurations of the printed WE; (b) amperometric responses to the additive 0.5 mM H_2O_2 at an applied potential of −0.15 V by the different configurations of the WE before immobilizing GOx (n = 6); (c) Nyquist diagram of the measured impedance of the different WE configurations in 5 mM potassium ferricyanide aqueous solution; (d) *in vitro* glucose detection results using the cylindrical flexible enzyme-electrode glucose biosensor (n = 6).

respectively, while both had synchronous heating before ultrasound treatment. Fig. 2(g) and (h) show the photos of the printed microelectrodes after ultrasound treatment (Ultrasonic Cleaners, 20 W, 20 kHz, 5 min). The printed microelectrodes on the substrate with surface modification show no difference after ultrasound treatment but come off of the substrate without modification. The results show printed microelectrodes' robust adhesion to the substrate with surface modification; robust adhesion is beneficial for electrochemical biosensors.

Characterization of the printed cylindrical electrochemical sensors

The *in vitro* experimental setup is shown in Fig. S2.† The measurement system consists of an electrochemical workstation (CHI 660E, Shanghai Chenhua Ltd. China) to supply the driving potential and to measure the output of the proposed sensor, a pump to provide different concentrations of the determinant in the reaction tank, and a computer to control and receive signals from the workstation. As shown in Fig. 3(a), the cyclic voltammetry characteristics of the printed flexible cylindrical electrochemical sensors with different configurations of the WE before immobilizing GOx were measured in 0.1 M PBS solution containing 1 mM H_2O_2. We used H_2O_2 to characterize the printed microelectrodes firstly because it would be produced during the glucose decomposition in the presence of GOx. The WE of PtNPs/rGO/Au exhibited the highest current peak, which was shown to be beneficial for electrochemical sensing. Each configuration of the WE was also tested using the amperometric technique. Fig. 3(b) shows the typical amperometric responses of various sensor configurations to successive increments of 0.5 mM H_2O_2 at an applied potential of −0.15 V. The electrochemical response increased as the H_2O_2 concentration increased, and all of the sensors demonstrated a good linearity from 0 to 4.5 mM H_2O_2 while the WE of PtNPs/rGO/Au exhibited the highest sensitivity. Fig. 3(c) shows the Nyquist plot of the electrochemical impedance spectra for different configurations of the WE. Here, 5 mM potassium ferricyanide in 0.1 M PBS was used as the determinant; voltages of 500 mV DC and 10 mV AC *versus* Ag/AgCl were applied between the WE and CE for frequencies in the range of 0.1 Hz to 100 kHz. Fig. 3(d) illustrates the measurement result from the proposed flexible enzyme-electrode glucose sensor after modifying GOx on the WE surface. This result indicates that the fabricated cylindrical flexible electrochemical enzyme-electrode sensor enables glucose detection in the range of 0–570 mg dL^{-1} with a detection limit of 3.54 mg dL^{-1} (S/N = 3) which exhibits the possibility for hypoglycemia ($\leq$50 mg dL^{-1}) detection.

After the electrochemical impedance spectroscopy test, we employed ZSimpWin to fit an equivalent circuit model which is shown in Fig. 4. The parameters of R_s, C_d, R_f, C_h, W, and R_t represent the solution impedance between the WE and RE, the capacitance of the double-layer capacitor of the WE, the finite layer diffusion impedance of the WE, the capacitance of the Helmholtz capacitor of the WE, the semi-infinite diffusion impedance of the WE, and the electron transfer resistance of the WE, respectively. Here, we care more about R_t because the sensitivity of a sensor is seriously affected by the electron transfer rate.[30] According to the measured electrochemical impedance spectra and the fitted equivalent circuit model, the R_t values for different WE configurations are calculated to be 4317 Ω cm^{-2} (Au), 982 Ω cm^{-2} (rGO/Au), and 63 Ω cm^{-2} (PtNPs/rGO/Au). The WE configuration of PtNPs/rGO/Au has the lowest electrochemical impedance which enhances the electron transfer rate to satisfy glucose monitoring at low levels of concentrations.

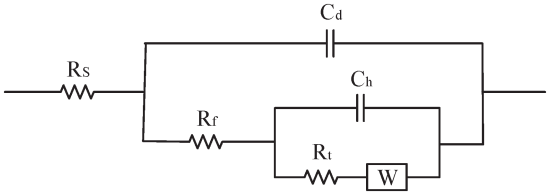

Fig. 4 Equivalent circuit model fitted by ZSimpWin.

In vivo animal experiment

After *in vitro* characterization of the fabricated cylindrical enzyme-electrode glucose biosensor, this kind of biosensor was tested *in vivo* through implantation in the subcutaneous tissue of a rat. The set up for the animal experiments is shown in Fig. S3.† The setup is similar to that for *in vitro* experiments while the reaction tank with PBS is substituted by the rat with ISF. The data was continuously recorded 30 min after the sensor was implanted to recover the physiological state of the rat. The measurement results of the implanted sensor and the commercial glucometer are shown in Fig. 5(a). This figure shows that the results obtained using the proposed cylindrical flexible enzyme-electrode biosensor exhibit great compliance with those obtained from the commercial glucometer. The implanted sensor detected the glucose concentrations in the ISF while the commercial glucometer measured the glucose in the caudate blood of the rat. Thus, the glucose concentrations recorded using the proposed sensor are delayed by about 25 min compared with those from the glucometer due to the physiological delay between the glucose concentrations in the ISF and those in blood.[31]

A one-point calibration model was used to calculate the glucose concentrations based on the obtained currents.[32] In detail, the sensitivity (0.354 nA/(mg dL^{-1})) of the sensor was obtained from the *in vitro* experimental results as shown in Fig. 3(d) while the background (−0.8546 nA/(mg dL^{-1})) should be calibrated based on the first point values of the current (recorded using an electrochemical workstation) and real glucose concentration (recorded using the commercial glucometer). Then, the *a* curve of glucose concentration variation *vs.* time was obtained. The values on this curve were

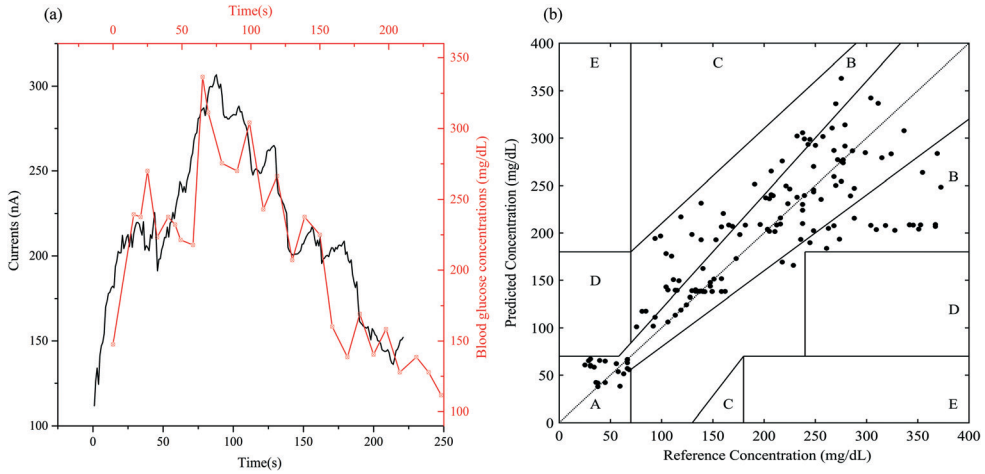

Fig. 5 (a) *In vivo* glucose measurement results using the fabricated cylindrical flexible enzyme-electrode sensor implanted into the subcutaneous tissue of the rat and the caudate blood glucose measured using the commercial glucometer; (b) plot of predicted glucose concentration *versus* reference glucose concentration on the Clarke error grid.

predicted as glucose concentrations while the values recorded using the commercial glucometer 25 min before were reference glucose concentrations. We could then obtain the Clarke error grid to evaluate the prediction accuracy as shown in Fig. 5(b).[33] The Clarke error grid consisted of five parts based on the probable treatment results according to the prediction glucose concentrations, and the definitions for the respective parts were as follows: A zone, clinically accepted accurate readings (no more than 20% deviation); B zone, moderate readings that are outside of 20% but would not lead to inappropriate treatment; C zone, readings that would lead to unnecessary treatment; D zone, readings that would result in a potentially dangerous failure when used in blood glucose correction; E zone, false readings that would cause confusing treatment for hypoglycemia and hyperglycemia. As illustrated in Fig. 5(b), all of the predicted values filled in the A and B zones (65% for A, 35% for B), which indicates that the proposed cylindrical flexible sensor can robustly and accurately predict the glucose concentrations in the physiological range. In particular, the fabricated sensor can accurately predict the glucose concentrations even under hypoglycemia conditions (less than 50 mg dL^{-1}) as shown in Fig. 5(b).

The solution soak is considered as the main factor for the adhesion between printed electrodes and the PEEK rod substrate. In our tests, several sensors were fabricated firstly and then characterized by *in vitro* and *in vivo* experiments. For both kinds of experiments, the sensors stably worked when soaked either in PBS with glucose in *in vitro* experiments or in the ISF in *in vivo* experiments. These results verify the robustness and reliability of the sensor which indicates that the fabricated sensor can completely satisfy the real application.

Conclusions

In this paper, a novel cylindrical flexible enzyme-electrode sensor was fabricated by rotated inkjet printing for implantable continuous glucose monitoring. APTES and MPTMS were used to modify the PEEK rod surface to make it hydrophilic and robustly adhesive to metals. Synchronous heating was used to prevent the droplets from flowing down along the cylindrical surface under gravity and in the direction of centrifugal forces during rotation. The two methods improve the printing quality of microstructures on micro cylindrical substrates. The proposed flexible sensor has a bigger WE surface and a 3D nanostructure on the WE, significantly improving the sensitivity to enable hypoglycemia detection. Furthermore, the fabricated cylindrical flexible electrochemical enzyme-electrode sensor enables glucose detection in the range of 0–570 mg dL^{-1} which meets the requirement in clinics. The *in vivo* rat experiment shows that the proposed cylindrical flexible enzyme-electrode sensor has the possibility for use in implantable continuous glucose monitoring in subcutaneous tissue. The proposed rotated inkjet printing method is promising for the microfabrication of flexible bioelectronics on arbitrary shapes of substrates. For the production line, a multi printhead array instead of only one printhead under laboratory conditions can be used to significantly improve the yield of manufacture of the sensor. And for the real application of the proposed cylindrical glucose sensor, an implantable detection circuit and a wireless signal generator could be designed to integrate with the sensor on the same cylindrical substrate to enable implantable continuous glucose monitoring and wireless signal transmission.

Live subject statement

SD rats were purchased from Beijing Vital River Laboratory Animal Technology Co., Ltd. All of the studies were performed following the appropriate guidelines (no. 20170201) and approved by the Animal Ethical and Welfare Committee of the Institute of Radiation Medicine Chinese Academy of Medical Sciences. The Affidavit of Approval of Animal Ethics and Welfare is shown in Fig. S4.†

Conflicts of interest

There are no conflicts to declare.

Acknowledgements

This work was supported by the National Natural Science Foundation of China (No. 81571766), the National Key R&D Program of China (No. 2017YFA0205103) and the 111 Project of China (No. B07014). We also thank Prof. Qian Wang, Prof. Yuan Lin and Mr. Jiawang Guo (Changchun Institute of Applied Chemistry Chinese Academy of Sciences) for their PtNP ink support.

References

1 Y. Y. Leung, J. C. Allen, L. W. Ang, J. M. Yuan and W. P. Koh, *Sci. Rep.*, 2017, **7**, 40671.
2 D. Aune, T. Feng, S. Schlesinger, I. Janszky, T. Norat and E. Riboli, *J. Diabetes Complications*, 2018, **32**, 501–511.
3 A. M. Gomez, G. E. Umpierrez, O. M. Munoz, F. Herrera, C. Rubio, P. Aschner and R. Buendia, *J. Diabetes Sci. Technol.*, 2015, **10**, 325–329.
4 A. Wood, D. O'Neal, J. Furler and E. I. Ekinci, *Intern. Med. J.*, 2018, **48**, 499–508.
5 S. N. Thennadil, J. L. Rennert, B. J. Wenzel, K. H. Hazen, T. L. Ruchti and M. B. Block, *Diabetes Technol. Ther.*, 2001, **3**, 357–365.
6 C. Cobelli, M. Schiavon, C. Dalla Man, A. Basu and R. Basu, *Diabetes Technol. Ther.*, 2016, **18**, 505–511.
7 H. Lee, Y. J. Hong, S. Baik, T. Hyeon and D. H. Kim, *Adv. Healthcare Mater.*, 2018, **7**, 1701150.
8 C. Chen, X. L. Zhao, Z. H. Li, Z. G. Zhu, S. H. Qian and A. J. Flewitt, *Sensors*, 2017, **17**, 182.
9 K. E. Kreider, B. I. Padilla and K. Pereira, *J. Nurse Pract.*, 2017, **13**, 228–234.
10 S. H. Lim, H. Y. Low and W. S. Tan, *J. Vac. Sci. Technol., B: Nanotechnol. Microelectron.: Mater., Process., Meas., Phenom.*, 2016, **34**, 011602.
11 W. M. Choi and O. O. Park, *Nanotechnology*, 2004, **15**, 1767–1770.
12 C. D. Petruczok and K. K. Gleason, *Adv. Mater.*, 2012, **24**, 6445–6450.
13 T. Wang, M. S. Hu, B. Yang, X. L. Wang and J. Q. Liu, presented in part at the *International Conference on Micro Electro Mechanical Systems*, Belfast, United Kingdom, 2018.
14 Y. J. Sun, H. Y. Li, Y. Lin, L. Niu and Q. Wang, *RSC Adv.*, 2016, **6**, 72519–72524.
15 M. Gao, L. H. Li and Y. L. Song, *J. Mater. Chem. C*, 2017, **5**, 2971–2993.
16 Z. Y. Zhan, J. N. An, Y. F. Wei, V. T. Tran and H. J. Du, *Nanoscale*, 2017, **9**, 965–993.
17 A. C. Hussein, *Master*, The University of British Columbia, 2010.
18 R. Walczak and K. Adamski, *J. Micromech. Microeng.*, 2015, **25**, 085013.
19 L. J. Deiner and T. L. Reitz, *Adv. Eng. Mater.*, 2017, **19**, 1600878.
20 C. M. Keum, I. H. Lee, H. L. Park, C. Kim, B. Lussem, J. S. Choi and S. D. Lee, *J. Appl. Phys.*, 2017, **121**, 244902.
21 Z. K. Gu, K. Wang, H. Z. Li, M. Gao, L. H. Li, M. X. Kuang, Y. S. Zhao, M. Z. Li and Y. L. Song, *Small*, 2017, **13**, 1603217.
22 B. Ando, S. Baglio, A. R. Bulsara, T. Emery, V. Marletta and A. Pistorio, *Sensors*, 2017, **17**, 1–11.
23 S. H. Ko, J. Chung, N. Hotz, K. H. Nam and C. P. Grigoropoulos, *J. Micromech. Microeng.*, 2010, **20**, 125010.
24 B. J. Polk, A. Stelzenmuller, G. Mijares, W. MacCrehan and M. Gaitan, *Sens. Actuators, B*, 2006, **114**, 239–247.
25 Y. Wang, T. T. Yang, J. C. Lao, R. J. Zhang, Y. Y. Zhang, M. Zhu, X. Li, X. B. Zang, K. L. Wang, W. J. Yu, H. Jin, L. Wang and H. W. Zhu, *Nano Res.*, 2015, **8**, 1627–1636.
26 Z. H. Pu, R. D. Wang, J. W. Wu, H. X. Yu, K. X. Xu and D. C. Li, *Sens. Actuators, B*, 2016, **230**, 801–809.
27 L. P. Ouyang, Y. C. Zhao, G. D. Jin, T. Lu, J. H. Li, Y. Q. Qiao, C. Q. Ning, X. L. Zhang, P. K. Chu and X. Y. Liu, *Biomaterials*, 2016, **83**, 115–126.
28 J. W. Wu, R. D. Wang, H. X. Yu, G. J. Li, K. X. Xu, N. C. Tien, R. C. Roberts and D. C. Li, *Lab Chip*, 2015, **15**, 690–695.
29 H. X. Zhang, Z. Li, B. Q. Wu, L. H. Dong, Y. J. Sun, Y. B. Leng and L. Wang, presented in part at the *2016 IEEE International Conference on Manipulation, Manufacturing and Measurement on the Nanoscale (3M-NANO)*, Chongqing, China, 2016.
30 Y. Y. Shao, J. Wang, H. Wu, J. Liu, I. A. Aksay and Y. H. Lin, *Electroanalysis*, 2010, **22**, 1027–1036.
31 K. Rebrin, N. F. Sheppard, Jr. and G. M. Steil, *J. Diabetes Sci. Technol.*, 2010, **4**, 1087–1098.
32 M. Takase, E. Takahashi, M. Murata, H. Ohnuki, K. Hibi, H. F. Ren and H. Endo, *Int. J. Environ. Anal. Chem.*, 2013, **93**, 125–139.
33 W. L. Clarke, S. Anderson, L. Farhy, M. Breton, L. Gonder-Frederick, D. Cox and B. Kovatchev, *Diabetes Care*, 2005, **28**, 2412–2417.